Analyst

Accepted Manuscript

ROYAL SOCIETY OF CHEMISTRY

www.rsc.org/analyst

A simple electrochemical platform based on pectin stabilized gold nanoparticles for picomolar detection of biologically toxic amitrole

Veerappan Mani[1], Rajkumar Devasenathipathy[1], Shen-Ming Chen[1*], V.S. Vasantha[2*], M. Ajmal Ali [3], Sheng-Tung Huang[1,4], Fahad M. A. Al-Hemaid[2]

[1]Electroanalysis and Bioelectrochemistry Lab, Department of Chemical Engineering and Biotechnology, National Taipei University of Technology, No.1, Section 3, Chung-Hsiao East Road, Taipei 106, Taiwan (R.O.C).

[2]Deaprtment of Natural Products Chemistry, School of Chemistry, Madurai Kamaraj University, Madurai, Tamil Nadu-625 021 , India.

[3]Department of Botany and Microbiology, College of Science, King Saud University Riyadh 11451, Saudi Arabia.

[4]Graduate Institute of Biomedical and Biochemical Engineering, National Taipei University of Technology, Taipei, Taiwan (Republic of China).

[1]*Corresponding Author. S.-M. Chen Fax: +886 2270 25238; Tel: +886 2270 17147, E-mail: smchen78@ms15.hinet.net

[2]*Corresponding Author. V.S. Vasantha Tel.: +91 452 245 8471x108; fax: +91 452 245 8449. E-mail: sivarunjan@gmail.com

Abstract

Amitrole is a biologically toxic nonselective herbicide which contaminates surface and ground waters at unprecedented rates. All reported modified electrodes detect amitrole within sub-micromolar to nanomolar levels which were based on the electro-oxidation of amitrole. Herein, we developed a new conceptual idea to detect picomolar concentration of amitrole based on calcium cross linked pectin stabilized gold nanoparticles (CCLP-GNPs) film modified electrode which was prepared by electrodeposition. When the electrochemical behavior of amitrole was investigated at CCLP-GNPs film, the reduction peak current of GNPs was linearly decreased as the concentration of amitrole increases. We have designed a determination platform based on the amitrole dependent decrease of GNPs cathodic peak. The described concept and high sensitivity of square wave voltammetry together facilitates great sensing ability; as a result the described approach able to reach low detection limit of 36 pM which surpassed the detection limits of existing protocols. The sensor presents good ability to determine amitrole in two linear concentration ranges: (1) 100 pM–1500 pM with detection limit of 36 pM; (2) 100 nM–1500 nM with detection limit of 20 nM. The preparation of CCLP-GNPs is simple, rapid and does not require any reducing agents.

Keywords: Nanobiotechnology, Amitrole, pesticides, electrocatalysis, gold nanoparticles, electrochemical sensor.

1. Introduction

For the past two decades, the use of pesticides has significantly increased in order to improve the agricultural productivity; however their residues at higher levels in the surface and ground waters cause severe health and environmental related problems[1-3]. Numerous pesticides were found to be present at exceeding concentrations in drinking water relative to the limit imposed by Environmental Protection Agency (EPA) which is a potential concern to human health[4]. Amitrole (3-amino-1,2,4-triazole) (**Fig. S1**) is a nonselective herbicide used in combination with other active agents to control wide range of weeds in agriculture areas. It also widely used as industrial herbicide to control weeds grown at roads and railway tracks [5, 6]. In 1971, the use of amitrole in food crops is banned by EPA, since it was proved as a carcinogenic agent for animals [7]. It is a potential pollutant to natural water resources due to its high solubility, polarity and low volatility in water [8, 9]. The European Economic Commission (EEC) directive

imposed an allowed upper limit of 0.1 μg L^{-1} for amitrole in drinking water. Therefore detection of amitrole at this concentration level is incredibly important to regulate amitrole toxicity in water resources [10, 11]. Various analytical methods such as liquid chromatography [10, 12], high performance liquid chromatography [5, 13], gas chromatography [14, 15], thin-layer chromatography [16] and capillary electrophoreses [17] have been developed for the determination of amitrole. However, these methods encountered difficulties due to the unfavorable properties of amitrole, such as high solubility in water, high polarity, low volatility, difficulty in extraction and preconcentration from aqueous samples, and poor solubility in organic solvents [10, 18]. On the other hand, electrochemical methods were proved to be more reliable and cost-effective for the determination of amitrole [19]. In relative to other methods, electrochemical methods have good advantages in terms of simplicity, direct use in point-of-care assays, simplicity and portability. However, electrochemical detection of amitrole at conventional bare electrodes suffers from drawbacks such as high overpotential and electrode fouling. These limitations can be overwhelmed by employing chemically modified electrodes, such as nafion/lead–ruthenium oxide pyrochlore [20], pre-anodized nontronite coated screen-printed electrode [21], electrochemically activated multiwalled carbon nanotubes (MWCNTs) paste electrode [7], ds-DNA decorated chitosan/MWCNTs [19], cobalt-phthalocyanine [18] , nickel nanoparticles [22]. Nyokong et al., have developed numerous phthalocyanine based modified electrodes for the determination of amitrole[8, 11, 23-25].

All these reports were based on direct electrochemical oxidation of amitrole at chemically modified electrodes. Despite their appreciable sensing performances, the limits of detections (LOD) are within sub-micromolar to nanomolar level. The state-of-the-art in amitrole detection is clearly indicating that one could not reach LOD less than nanomolar by studying the direct oxidation of amitrole. In other words, different approach should be developed to drive the LOD beyond nanomolar range. By keeping this requirement as objective, we have developed a new sensing approach based on calcium cross linked pectin (CCLP) stabilized gold nanoparticles (GNPs) for the ultrasensitive detection of amitrole. The conceptual idea of this work is to study the amitrole concentration dependent cathodic peak current of GNPs. The described approach detects picomolar concentration of amitrole with LOD of 36 pM which surpassed the LODs of existing methods. Pectin (polygalacturonic acid) is a naturally occurring biopolymer present at the cell walls of plants, while CCLP is a gel prepared by mixing pectin with calcium ions [26]. The

CCLP was employed as scaffold to prepare stable GNPs on glassy carbon electrode surface (GCE) through simple and rapid electrodeposition process[27]. The preparation of the CCLP-GNPs involves short time, simple and easily reproducible procedures and does not require hazardous reducing agents. The main aim of this work is to explore a new electrochemical approach for the ultra-sensitive detection of amitrole.

2. Experimental

2.1 Reagents and apparatus

Pectin (from citrus peel), calcium chloride, $HAuCl_4$ and all other chemicals were purchased from Sigma-Aldrich and used without any purification. The supporting electrolyte used for the electrochemical studies was 0.05 M phosphate buffer. The GCE surface was polished with 0.05 µm alumina slurry using a Buehler polishing kit, then washed with water and dried at ambient conditions. The pre-cleaned GCE was employed for the electrodeposition of CCLP stabilized GNPs.

The electrochemical measurements were carried out using CHI 611A electrochemical work station. Electrochemical studies were performed in a conventional three electrode cell using modified GCE as a working electrode (area 0.071 cm^2), saturated Ag|AgCl (saturated KCl) as a reference electrode and Pt wire as a counter electrode. Scanning electron microscopy (SEM) studies and Energy-dispersive X-ray (EDX) spectra were carried out using Hitachi S-3000 H scanning electron microscope and HORIBA EMAX X-ACT (Sensor + 24V=16 W, resolution at 5.9 keV) respectively. The UV–Visible absorption spectroscopic measurements were performed using Hitachi U-3300 spectrophotometer (EquipNet, Inc., USA). Powder X-ray diffraction (XRD) studies were performed in a XPERT-PRO (PANalytical B.V., The Netherlands) diffractometer using Cu Kα radiation (k =1.54 Å). Electrochemical impedance spectroscopy (EIS) studies were carried out using EIM6ex ZAHNER (Kroanch, Germany).

2.2 Electrodeposition of CCLP stabilized GNPs on GCE

CCLP stabilized GNPs were electrodeposited on GCE surface by following our previously reported procedure [27]. Briefly, 10 mg of calcium chloride dihydrate and 5 mg of pectin were added to 5 ml of 0.1 M KNO_3 and ultrasonicated for 15 min to get a uniform gel

denoted as CCLP. The as-prepared CCLP (3 mg mL^{-1}) and $HAuCl_4$ (0.33 mg mL^{-1}) were mixed and ultrasonicated for 15 min and transferred to an electrochemical cell. The electrodeposition was carried out by recording cyclic voltammetry at the potential range between 1.40 V and –1.40 V for 10 cycles. The scan rate was applied as 50 mV s^{-1}. After the completion of electrodeposition, the CCLP stabilized GNPs (CCLP-GNPs) film modified GCE was washed with water and dried at ambient conditions. A cleaning procedure is employed to carry out repeatability and stability studies. Before making a new detection on the same electrode, the electrode was cleaned by running five consecutive cyclic voltammogram at the potential range of −1.0 to 1.0 V in 0.1 M H_2SO_4. Subsequently, the electrode was rinsed with water and used for new detection.

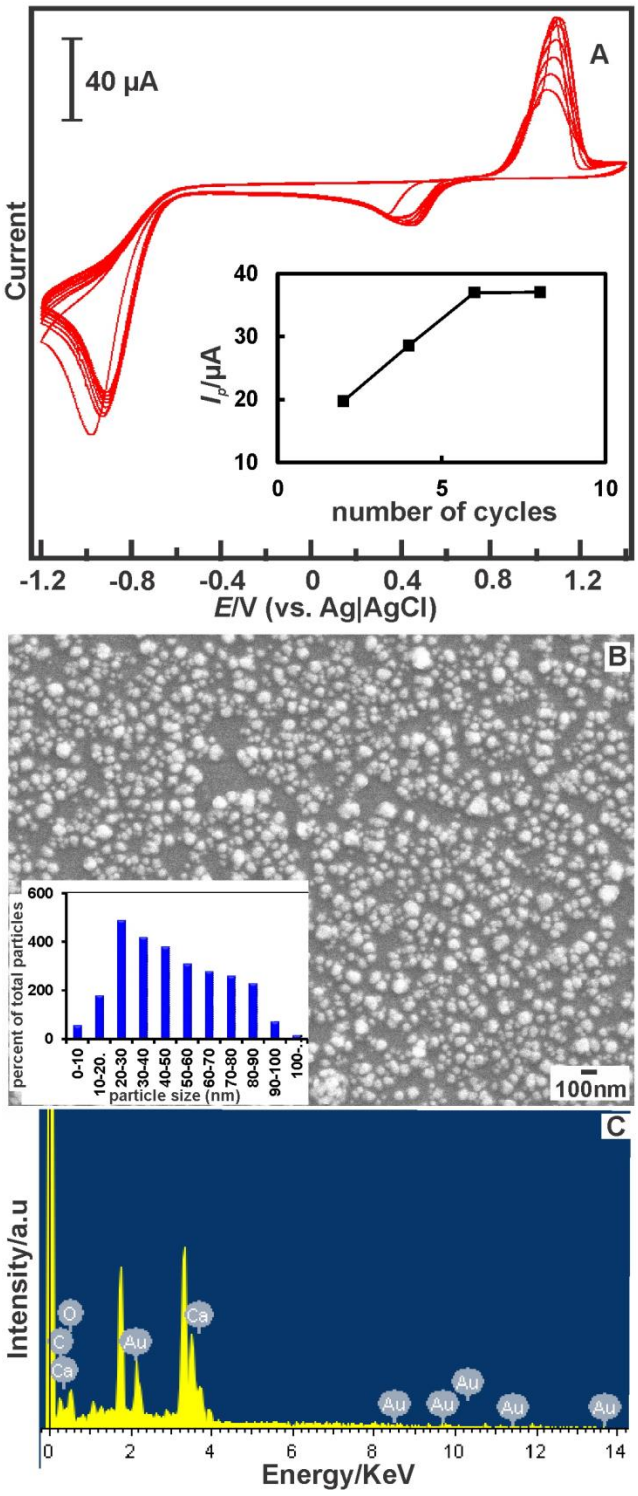

Fig. 1 (A) Electrodeposition of CCLP stabilized GNPs on GCE in 0.1 M HCl containing CCLP-$HAuCl_4$ for 6 cycles. Scan rate = 25 mV s^{-1}. Inset: Optimization of number of cycles for

electrodeposition. SEM image (B) of CCLP-GNPs, inset: particle size distribution plot. EDX spectrum (C) of CCLP-GNPs.

3. Results and Discussion

3.1 Characterization of CCLP-GNPs

F**ig. 1A** presents the cyclic voltammograms (CVs) recorded for the electrodeposition of CCLP-GNPs. A sharp reduction peak observed at the potential of + 0.51 V was assigned to the reduction of GNPs, while a broad peak observed at + 1.0 V was assigned to the oxidation of GNPs. Additionally, typical hydrogen evolution peak was observed at – 0.85 V in the forward scan. During continuous cycling, the growth of reduction and oxidation peak currents validated the successful formation of GNPs [28]. The optimum amount of GNPs required to obtain maximum electrocatalysis had been optimized by tuning the number of deposition cycles; the oxidation of amitrole at CCLP-GNPs/GCE was tested at different electrodeposition cycles ranging from 1 to 8 (**Inset to Fig. 1A**). The maximum response was observed at 6 cycles and hence 6 cycles was used as optimized cycles for electrodeposition of CCLP-GNPs.

The SEM image of CCLP-GNPs depicts uniform decoration of GNPs within the interconnected network of CCLP (**Fig. 1B**). The nanoparticles sizes are ranging from 15 to 50 nm evident from the particle size distribution plot (inset to Fig. 1B). The EDX spectrum of CCLP-GNPs presents signals for carbon, oxygen, calcium and gold with weight percentage of 15.10, 35.12, 16.08 and 33.70%, respectively (**Fig. 1C**). The presence of high weight percentage of gold indicates the high loading of GNPs into the CCLP matrix. The UV-Visible spectrum of CCLP-GNPs featured with a typical absorption peak at the wavelength of 560 nm evident for the successful formation of GNPs[29] (**Fig. S2A**). The XRD pattern of the CCLP-GNPs displays four important diffraction peaks at 2θ angles of 38.72°, 44.52°, 64.64° and 77.95° assigned to (111), (200), (220) and (311) reflections, respectively and the pattern is consistent with that of face-centered cubic structure of metallic GNPs (JCPDS, card no. 04-0784) (**Fig. S2B**).

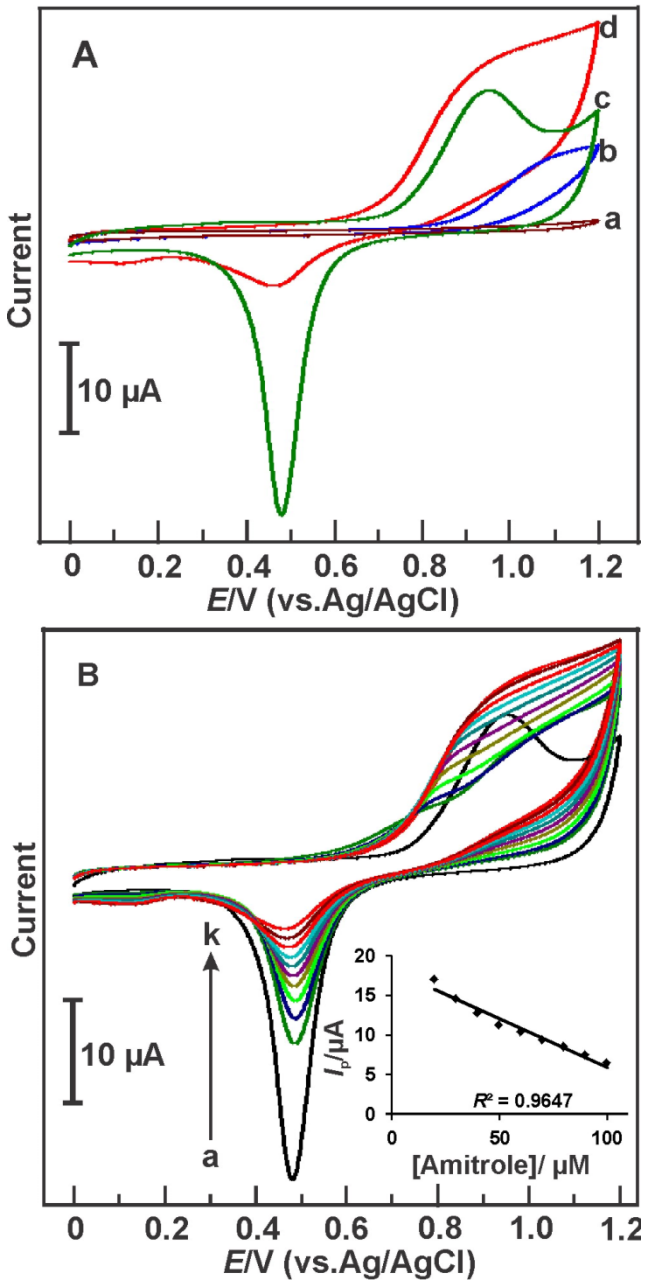

Fig. 2 (A) CVs obtained at bare GCE in the absence (a) and presence of 100 μM amitrole (b) and CVs obtained at CCLP-GNPs in the absence (c) and presence of 100 μM amitrole (d) in phosphate buffer (pH 7) at the scan rate of 50 mVs^{-1}. (B) CVs obtained at CCLP-GNPs in the absence (a) and presence of amitrole with the concentration ranging from 10 μM to 100 μM (b-k). Inset: Plot of I_{pc} vs. [Amitrole].

3.2 Electrochemical detection of amitrole

The electrochemically active real surface areas of GCE and CCLP-GNPs/GCE were assessed using $K_3[Fe(CN)_6]$ as a model redox mediator, while Randles–Sevcik equation was used to calculate the areas[30]. The electrochemically active surface areas of GCE and CCLP-GNPs/GCE were calculated to be 0.079 cm^2 and 0.141 cm^2 respectively. The real area of the CCLP-GNPs/GCE is nearly twice that of GCE which might be due to the large surface, porosity and presence of surface roughness. **Fig. 2A** displays the CVs obtained at bare GCE and CCLP-GNPs/GCE in the absence and presence of amitrole. The CVs were carried out in phosphate buffer (pH 7) at the scan rate of 50 mV s^{-1}. Bare GCE exhibits sluggish electrocatalytic ability to amitrole; it showed broad anodic peak at large overpotential (+ 1.10 V) for the oxidation of amitrole. Comparatively, the CCLP-GNPs/GCE exhibits good electrocatalytic ability evident from the observation of anodic peak at + 0.90 V (onset potential ≈ 0.58 V). As the concentration of amitrole increases, the peak current corresponding to oxidation of amitrole was increased; however, at high concentrations it was almost disappeared and a hump like broad peak was obtained at 1.0 V (Fig. 2B). As mentioned in the introduction section, although the direct oxidation of amitrole is well-established for the determination of amitrole, it grants poor LODs [7, 8]. Interestingly, the peak current responsible for the reduction of GNPs (I_{pc}) observed at + 0.51 V (explained in section 3.1) is significantly decreased in the reverse scan. The interesting aspect is the linear decrease in I_{pc} with respect to the concentration of amitrole which must be due to adsorption of amitrole on GNPs (**inset to Fig. 2B**). The adsorptions of amitrole on the gold nanoparticles take place by self-assembly through the special affinity between amines (present on the amitrole) and GNPs. The time required to the amitrole adsorption was optimized. The adsorption was tested for the time duration of 1 min, 2 min, 3 min and 4 min; the optimum adsorption was obtained at 2 min and therefore we used 2 min interval between each analysis. The stability of I_{pc} in the absence of amitrole was investigated in order to support our claim. 250 continuous CVs were performed at CCLP-GNPs in phosphate buffer (pH 7) in the absence of amitrole. The initial I_{pc} is almost retained even after 250 consecutive CVs with only 5.3% decrease. Accordingly, we confirmed that the I_{pc} is stable in the absence of amitrole; while linearly decreases as concentration of amitrole increases.

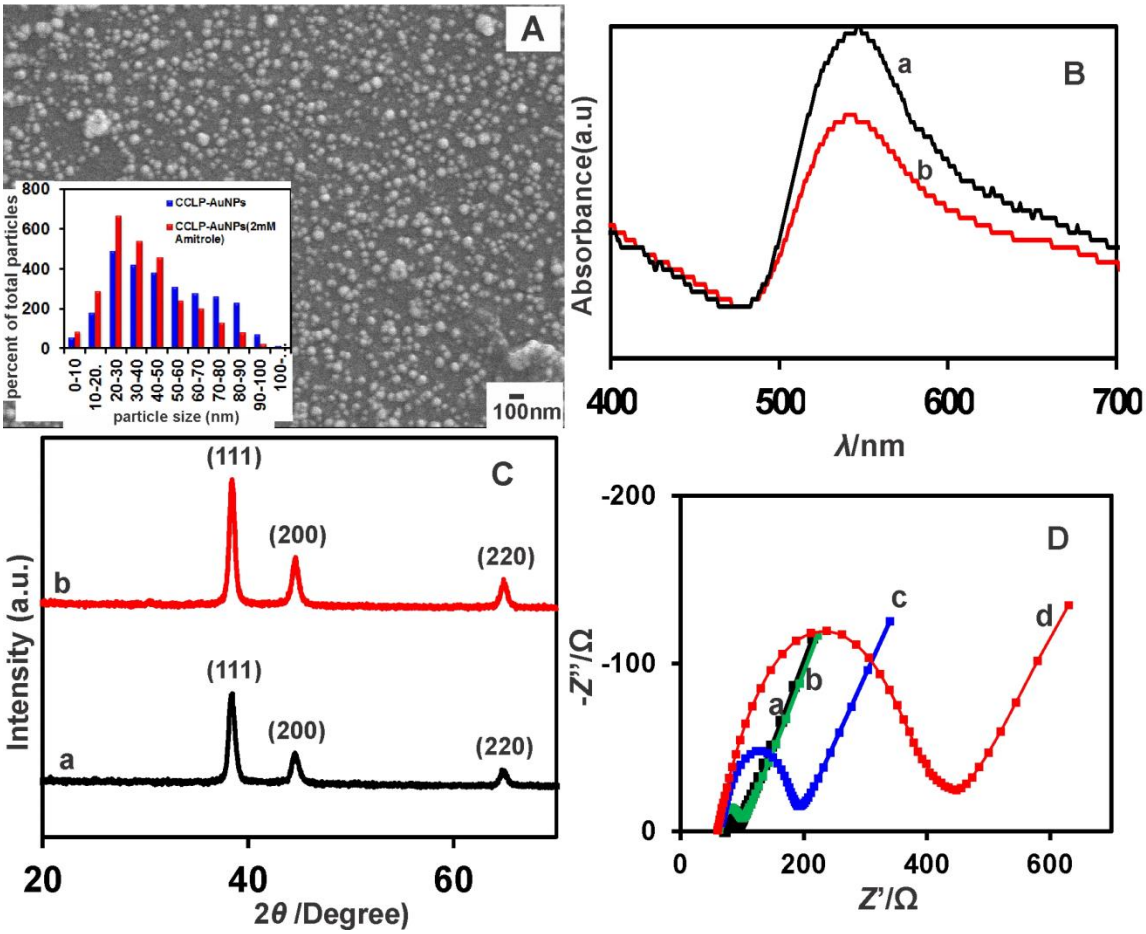

Fig. 3 (A) SEM image of CCLP-GNPs in the presence of 2 mM of amitrole, inset: particle size distribution plot. (B) UV-Vis spectrum and XRD pattern of CCLP-GNPs/GCE in the absence (a) and presence of 2 mM amitrole (b). (D) EIS spectra of CCLP- GNPs in the absence (a) and presence of 10 µM (b), 100 µM (c) and 500 µM (d) amitrole.

In order to investigate the reason for decrease in I_{pc}, we have carried out SEM, UV-vis spectra, EIS and XRD pattern of CCLP-GNPs in the absence and presence of amitrole (**Fig. 3**). The SEM images of CCLP-GNPs in the absence (**Fig. 1B**) and presence of amitrole **(Fig. 3A**) are different. In the presence of amitrole (100 µM), the morphology of CCLP-GNPs shows spherical shaped particles with more uniformity. Notably, the particle sizes were significantly decreased after the adsorption of amitrole as represented by the particles size distribution plot (**inset to Fig. 3A**). Here, the primary amino group present in the amitrole has special affinity to the GNPs which leading to the self-assembly of amitrole on the gold nanoparticles[27, 31-33] (**scheme 1**). The remaining triazo–electron centers of neighboring adsorbed amitrole molecules may experience

repulsive forces due to the lone pair-lone pair repulsion and this repulsive force may prevent the aggregation of GNPs and hence the GNPs size decreases (**scheme 1**). The UV-Visible spectroscopy (**Fig. S2A and Fig. 3B**) and XRD studies (**Fig. S2B and Fig. 3C**) were also supported for the particles size decrease in the presence of amitrole.

Furthermore, we have carried out EIS studies in the presence of different concentration of amitrole (**Fig. 3D**). The electron transfer resistance (R_{ct}) at electrode surface is equal to the semicircle diameter, which can be used to describe the interface properties of the electrode. As observed from figure, the diameter of semicircle increased when concentration of amitrole was linearly increased as the concentration of amitrole increases (a= 0, b=10, c=100 and d= 500 µM). It is well known fact that most organic molecules such as amitrole are poor electrical conductor. Hence, the linear increase in R_{ct} should be due to the electron transfer hindrance by the adsorption of amitrole molecules on the CCLP-GNPs surface. Based on the above results, a plausible mechanism has been derived and given as **scheme 1.**

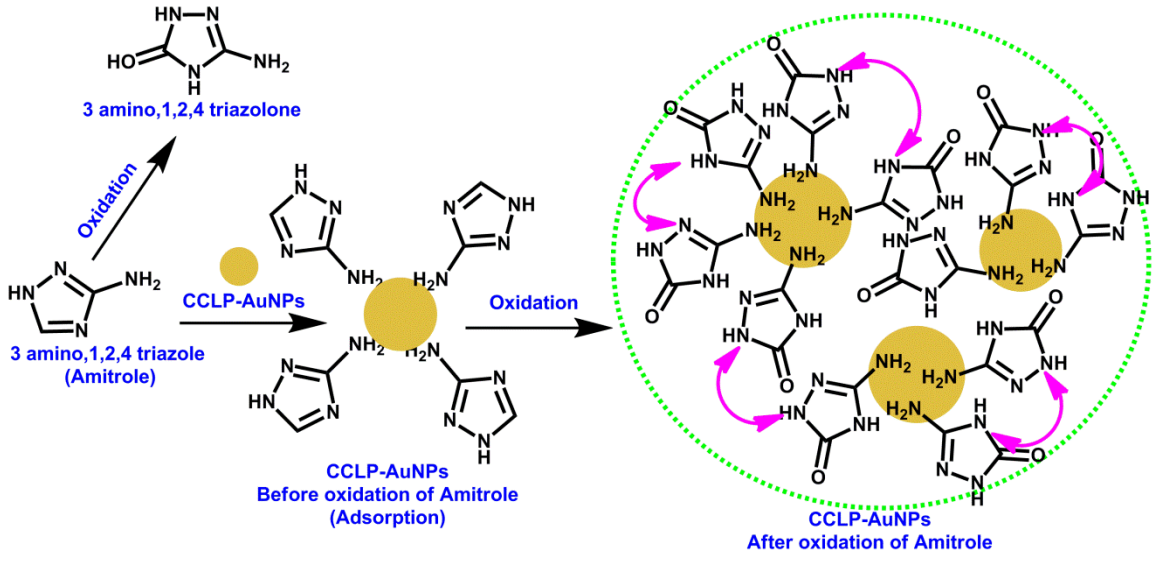

Scheme 1. Possible mechanistic pathway for the determination of amitrole through GNPs size induced oxidation.

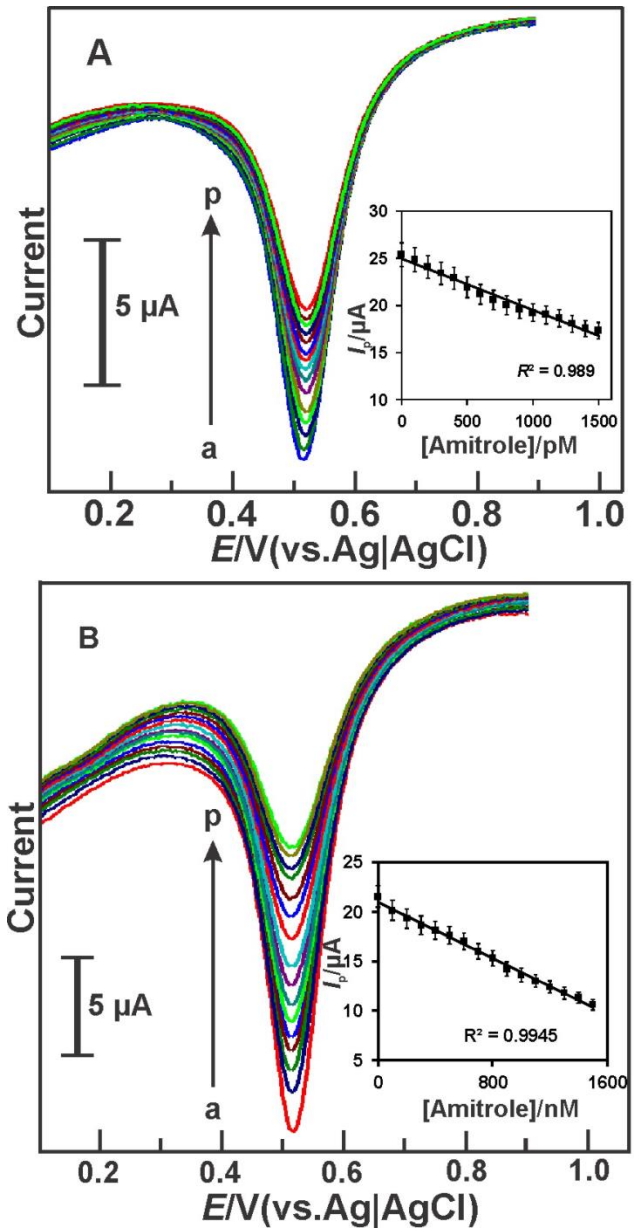

Fig. 4 (A) SWVs obtained at CCLP-GNPs/GCE in the absence (a) and presence of amitrole ranging from 100 nM to 1500 nM (b to p; each addition of 100 nM) in phosphate buffer (pH 7). Inset: Calibration plot, [Amitrole] vs. peak current, I_p (µA) = – 5.50 [amitrole] (nA/pM) + 24.93. (B) SWVs obtained at CCLP-GNPs/GCE in the absence (a) and presence of amitrole ranging from 100 pM to 1500 pM (b-p; each addition 100 pM) in phosphate buffer (pH 7). Inset: Calibration plot, [Amitrole] vs. peak current; I_p (µA) = – 0.0071 [amitrole] (µA/nM) + 20.985.

3.3 Determination of amitrole by square wave voltammetry

Fig. 4A presents the square wave voltammograms (SWVs) obtained at CCLP-GNPs/GCE in the absence (curve a) and presence of amitrole (each addition of 100 pM; b to p, 100 pM to 1500 pM) in phosphate buffer (pH 7). The SWV records sensitive responses to the each addition of amitrole with an obvious decrease in the I_{pc}. A linear calibration plot between I_{pc} and [amitrole] exhibits good linearity with slope of – 5.50 nA/pM (**inset to Fig. 4A**). The working linear range and sensitivity of the sensor were estimated to be 100 pM–1500 pM and 77.46 $nApM^{-1}$ cm^{-2}, respectively. The LOD value was calculated to be 36 pM (S/N=3). Another linear range was observed at higher concentration range from 100 nM–1500 nM (**Fig. 4B)**. The linear range and sensitivity of the second range was estimated to be 100 nM–1500 nM and 100 $nA\ nM^{-1}\ cm^{-2}$ (**inset to Fig. 4B**). The LOD at this linear range was calculated to be 20 nM (S/N=3). Here, the sensitivity observed at the higher concentration range (**inset to Fig. 4B**) is relatively lower than that observed at lower concentration range (**inset to Fig. 4A**) which should be due to the occurrence of substrate inhibition effects at higher concentration of amitrole.[34] The important analytical parameters of the sensor, such as LOD, linear range and sensitivity have been compared with previous reports (**Table 1**). As shown in the table, generally all the reported modified electrodes able to detect micromolar concentration of amitrole; only carbon paste electrode modified with iron phthalocyanine nanoparticles shows low LOD (≈3.62 nM). However, our newly developed approach exhibits LOD of 36 pM which is significantly lower than the previously published reports. Therefore, we strongly believe that the proposed approach is a promising way to direct the amitrole sensor design into new route aiming towards real-time ultrasensitive detection of amitrole.

Table 1. Comparison of analytical parameters for the determination of amitrole at CCLP-GNPs film modified electrode with other films modified electrodes

Electrode	Method	LOD	Linear range	Sensitivity	Ref.
[a]MWCNT paste electrode	[g]ASV	0.6 µM	0.8–7 .0 µM	-	[7]
[b]FeTAPc/BPPGE-MWCNT	[h]CA	0.5 nM	–	8.80 µA nM^{-1}	[11]
[c]CoTCPc–EA–SWCNT	CA	0.1 µM	10–160 µM	0.76 A M cm^{-2}	[24]
[d]CoTOBPc–SWCNT	CA	–	1.0–30µM	1.13 A M cm^{-2}	[25]

[e]FePc-CPE	CA	3.62±0.11nM	1–12 nM	3.44μA nM^{-1}	[8]
[f]FeTAPc-SWCNT dendrimer	CA	0.215 μM	63–100 μM	0.6603 μA μM^{-1}	[23]
Nafion/lead–ruthenium oxide pyrochlore	[i]SWV	0.38 μM	30–250 μM	0.073 μA μM^{-1}	[20]
CCLP-GNPs	SWV	36 pM; 20 nM	100–1500 pM, 100–1500 nM	0.075 μApM^{-1} cm^{-2} 0.1 μA$nM^{-1}cm^{-2}$	This work

[a]MWCNT= multiwalled carbon nanotubes, [b]FeTAPc/BPPGE-MWCNT= iron(II) tetra-aminophthalocyanine/basal planepyrolytic graphite electrode-MWCNT, [c]CoTCPc–EA–SWCNT= cobalt (II) tetracarboxylphthalocyanine-ethylene amine- single-walled carbon nanotubes, [d]CoTOBPc–SWCNT= 2,(3)-tetra-(4-oxo-benzamide)phthalocyaninato cobalt (II)–single walled carbon nanotube, [e]FePc-CPE= Iron (II) phthalocyanine nanoparticles-carbon paste electrode, [f]FeTAPc-SWCNT= Iron (II) tetraaminophthalocyanine-single walled carbon nanotube, [g]ASV=Adsorptive Stripping Voltammetry, [h]CA=Chronoamperometry, [i]SWV= Square Wave voltammetry.

Selectivity of the described sensor to the determination of amitrole (500 pM) has been investigated in the presence of variety of likely interferences. 1000 folds excess concentration (500 nM) of Na^+, K^+, Ca^{2+}, Mg^{2+}, Ba^{2+}, Fe^{2+}, Co^{2+}, Ni^{2+}, F^-, Cl^-, Br^-, I^- and $(COO)_2^{2-}$ and 100 folds excess concentration (50 nM) of trazine, atraton, 2-hydroxy atrazine and ametryn were tested (**Fig. S3**). The aforementioned species unable to follow the novel pathway specially designed for the determination of amitrole and hence they don't have any detectable signals (less than 5%) at CCLP-GNPs/GCE. Therefore, we infer that CCLP-GNPs/GCE has the ability to selectivity detect amitrole through the proposed mechanistic pathway.

3.4 Stability, repeatability, reproducibility and practicality

The stability of the modified electrode to detect amitrole has been tested by monitoring the I_{pc} of the CCLP-GNPs/GCE in the presence of amitrole (500 pM). Only 7.58% of the initial I_{pc} was decreased even after 100 CV cycles indicating the stable response of the CCLP-GNPs/GCE. In order to determine storage stability of the electrode, the I_{pc} obtained responsibe for amitrole (500 pM) was recorded every day. The electrode was stored in at 4°C when not in

use. Even after one month stroge period, the electrode presents well defined response to detect amitrole without any shift in the peak potential. 94.82% of the initial I_p was retained over one month storage validated appreciable storage stability. Repeatability and reproducibility of the CCLP-GNPs/GCE were evaluated in phosphate buffer (pH 7) containing amitrole (500 pM). The sensor exhibits appreciable repeatability with relative standard deviation (R.S.D) of 3.64% for 5 repeatitive measurements carried out using single CCLP-GNPs/GCE. Additionaly, the sensor exhibits acceptable reproducibility of 3.44% for the five independent measurements carried out in five different electrodes. In order to evaluate practicality of the sensor, water samples such as tap water, river water were employed. The spiked amitrole concentrations are, 100 and 200 pM. As shown in **table S1**, the proposed method has shown good recoveries ranging from 97.5 to 103.3% for the detection of amitrole revealing the practical feasibility of the described approach.

4. Conclusions

In summary, we set-up a ultrasensitive electrochemical platform for the determination of picomolar concentration of amitrole at CCLP-GNPs film. A new conceptual idea to study the concentration dependent cathodic peak of GNPs rather than direct oxidation of amitrole was proposed and studied. The possible mechanism for the decrease of I_{pc} in the presence of amitrole was derived and investigated by various methods. Using SWVs, the sensor exhibited outstanding sensing ability to determine amitrole in two ranges: (1) 100 pM–1500 pM with LOD of 36 pM; (2) 100 nM–1500 nM with LOD of 20 nM. The achieved LOD (≈36 pM) surpassed the LODs of existing methods. The practical feasibility of the sensor was demonstrated in water samples. The excellent attributes of the proposed approach holds great promise to direct amitrole sensor design into new pathway for the real-time detection of amitrole.

Acknowledgement

This project was supported by the Ministry of Science and Technology and the Ministry of Education of Taiwan (Republic of China). Dr. Veerappan Mani greatfully acknowledge the National Science Council, Taiwan for the postdoctoral fellowship (NSC 103-2811-M-027-002). Research supported by the King Saud University, Deanship of Scientific Research, College of Science, and Research Center.

References

1. M. Fontecha-Cámara, M. López-Ramón, L. Pastrana-Martínez and C. Moreno-Castilla, *Journal of hazardous materials*, 2008, **156**, 472-477.
2. W. Ritter, *Journal of Environmental Science & Health Part B*, 1990, **25**, 1-29.
3. R. Wauchope, *Journal of environmental quality*, 1978, **7**, 459-472.
4. J. Hetrick, R. Parker, R. Pisigan Jr and N. Thurman, *Briefing Document for a Presentation to the FIFRA Scientific Advisory Panel (SAP)*, 2000.
5. Y. Sun, P. F. Liu, D. Wang, J. Q. Li and Y. S. Cao, *Journal of agricultural and food chemistry*, 2009, **57**, 4540-4544.
6. L. Agnolucci, F. D. Vecchia, R. Barbato, V. Tassani, G. Casadoro and N. Rascio, *Journal of plant physiology*, 1996, **147**, 493-502.
7. M. Chicharro, E. Bermejo, M. Moreno, A. Sánchez, A. Zapardiel and G. Rivas, *Electroanalysis*, 2005, **17**, 476-482.
8. M. Siswana, K. I. Ozoemena and T. Nyokong, *Talanta*, 2006, **69**, 1136-1142.
9. T. Oesterreich, U. Klaus, M. Volk, B. Neidhart and M. Spiteller, *Chemosphere*, 1999, **38**, 379-392.
10. J. Dugay and M.-C. Hennion, *TrAC Trends in Analytical Chemistry*, 1995, **14**, 407-414.
11. M. Siswana, K. I. Ozoemena and T. Nyokong, *Sensors*, 2008, **8**, 5096-5105.
12. M. Kuster, M. L. de Alda and D. Barceló, *Mass spectrometry reviews*, 2006, **25**, 900-916.
13. Y. Sun, L. Luo, F. Wang, J. Li and Y. Cao, *Analytical and bioanalytical chemistry*, 2009, **395**, 465-471.
14. B. V. Pepich, B. Prakash, M. M. Domino, T. A. Dattilio, D. J. Munch and E. K. Price, *Environmental science & technology*, 2005, **39**, 4996-5004.
15. J. Van der Poll, M. Vink and J. Quirijns, *Chromatographia*, 1990, **30**, 155-158.
16. J. Pribyl, F. Herzel and G. Schmidt, *FRESENIUS ZEITSCHRIFT FUR ANALYTISCHE CHEMIE*, 1978, **289**, 81-85.
17. M. Chicharro, M. Moreno, E. Bermejo, S. Ongay and A. Zapardiel, *Journal of Chromatography A*, 2005, **1099**, 191-197.
18. M. Chicharro, A. Zapardiel, E. Bermejo, M. Moreno and E. Madrid, *Analytical and bioanalytical chemistry*, 2002, **373**, 277-283.

19. A. A. Ensafi, M. Amini and B. Rezaei, *Colloids and Surfaces B: Biointerfaces*, 2013, **109**, 45-51.
20. J.-M. Zen, A. Senthil Kumar and M.-R. Chang, *Electrochimica Acta*, 2000, **45**, 1691-1700.
21. J.-M. Zen, H.-P. Chen and A. Senthil Kumar, *Analytica chimica acta*, 2001, **449**, 95-102.
22. A. Maringa, T. Mugadza, E. Antunes and T. Nyokong, *Journal of Electroanalytical Chemistry*, 2013, **700**, 86-92.
23. T. Mugadza and T. Nyokong, *Electrochimica Acta*, 2010, **55**, 2606-2613.
24. T. Mugadza and T. Nyokong, *Synthetic Metals*, 2010, **160**, 2089-2098.
25. T. Mugadza, Y. Arslanoğlu and T. Nyokong, *Electrochimica Acta*, 2012, **68**, 44-51.
26. S. F. Ahrabi, G. Madsen, K. Dyrstad, S. A. Sande and C. Graffner, *European journal of pharmaceutical sciences*, 2000, **10**, 43-52.
27. R. Devasenathipathy, V. Mani, S.-M. Chen, D. Arulraj and V. Vasantha, *Electrochimica Acta*, 2014, **135**, 260-269.
28. M. Rajkumar, S.-C. Chiou, S.-M. Chen and S. Thiagarajan, *Int. J. Electrochem. Sci*, 2011, **6**, 3789-3800.
29. J. Heo, D.-S. Kim, Z. H. Kim, Y. W. Lee, D. Kim, M. Kim, K. Kwon, H. J. Park, W. S. Yun and S. W. Han, *Chemical Communications*, 2008, 6120-6122.
30. C. Liu, H. Zhang, Y. Tang and S. Luo, *Journal of Materials Chemistry A*, 2014, **2**, 4580-4587.
31. A. J. Jeevagan and S. A. John, *RSC Advances*, 2013, **3**, 2256-2264.
32. K. S. Lokesh, V. Narayanan and S. Sampath, *Microchimica Acta*, 2009, **167**, 97-102.
33. G. Liu, E. Luais and J. J. Gooding, *Langmuir*, 2011, **27**, 4176-4183.
34. V. Mani, B. Dinesh, S.-M. Chen and R. Saraswathi, *Biosensors and Bioelectronics*, 2014, **53**, 420-427.